# Foam drainage: A film contribution?

V. Carrier, S. Destouesse, and A. Colin

*CRPP, Avenue Dr. A. Schweitzer, 33600 Pessac, France*

We have measured the steady drainage of foams of various surfactants, varying the size of the parietal plateau borders from 0.24 to 2.4 mm. We report an evolution of the power laws of drainage with the bubble size, which cannot be explained by the most recent developments of the drainage theory. We believe that one reason for the disagreement between the existing theory and our data is the passage of liquid through the films, from nodes to nodes. Film thickness measurements *in situ* show that the films are swollen, up to 2 $\mu$m and more. Films, usually neglected, may then have an important contribution to drainage by increasing noticeably the volume of the regions where the liquid flows.

## I. INTRODUCTION

Foam is the name given to dispersion of gas into a liquid or a solid. The most common liquid foams are concentrated dispersions of air into water, resulting from the compaction of air bubbles due to gravity.

These foams are found in everyday life in soaps, shampoos, detergents, cooking, and beverages, as well as in industrial applications such as fire fighting, foam chromatography, and flotation. In these last applications, the kinetics of flow of the water between the foam bubbles are critical: these kinetics rule the time after which the foam will have released most of its water. This phenomenon of water flowing inside the foam is called drainage.

This drainage has been studied thoroughly for 40 years now, both theoretically [1–13] and experimentally [1,4,5,7,10,12,13]. It has been shown noticeably that the water is mainly contained and is mainly circulating inside a continuous network of interconnected channels. These channels, called plateau borders, are formed at the meeting of three soap films inside the foam and join fourfold in regions called nodes. It has been shown also that the flow is driven by gravity and capillary forces, and is slowed down by viscous forces either in channels or in nodes. The main present questions rely on the description of this viscous force.

In this study, we carried out an experimental work to test the most recent models of drainage. As compared to existing experimental studies, we have accomplished measurements on enlarged values of flow rate and liquid fraction, and for an enlarged range of bubble size. We thus show that the existing models are unable to describe our results. We put into evidence a regime where the flow is enhanced, noticeably for high liquid fractions and fine foams. We finally demonstrate by measuring the thickness of films *in situ* in draining foams that the soap films, which have always been neglected in drainage, may contribute to the flow, by increasing the volume of the regions where the liquid flows.

We present first the theory we used to analyze our data, next the experimental methods of drainage investigation, followed by their results and finally the measurements of film thickness.

## II. THEORETICAL BACKGROUND

We present here the most recent developments of the drainage theory, taking into account the contribution of Koehler *et al.* [12,13] together with those of Leonard and Lemlich [4], and Desaï and Kumar [2]. The following modeling is done.

The foam is supposed to be sufficiently monodisperse to be treated as an assembly of bubbles of same behavior, but sufficiently polydisperse as to neglect correlation in orientation and position of the bubbles.

The bubbles are modeled as Kelvin cells.

The films do not intervene in drainage and are of negligible thickness.

All the surfaces are considered saturated with surfactants, with no concentration gradients.
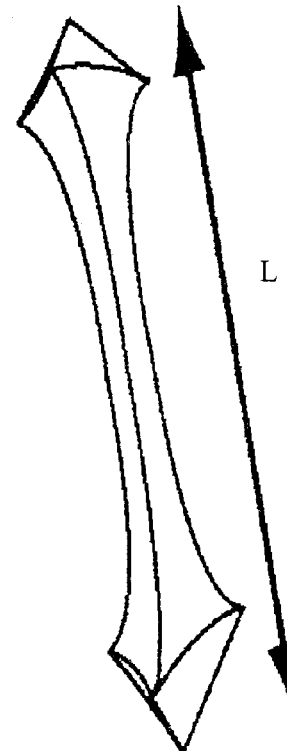


FIG. 1. Dogbone shaped.

In this modeling, the foam can be seen as a statistical assembly of the elementary cell that Koehler *et al.* named "dogbone shaped" (Fig. 1) which is a plateau border with a quarter of a node at each end. Two length scales define this element; the total length $L$, and the curvature radius of the plateau border $r$. We divide this element into a straight part of length $L$-$\alpha r$ and section $a = \delta_a r^2$, which we will call plateau border, and a node part of volume scaling as $r^3$. $\alpha$ is a geometrical constant and can be approximated as $4\cos(109°28'/2)$, and $\delta_a$ equals $\sqrt{3} - \pi/2$. Applying the Stokes equation on this element, we get

$$\int_{V_{PB}+V'_N}(-\vec{\nabla}P+\rho\vec{g})dV$$
$$= -\eta\left(\int_{V_{PB}}\Delta_l\vec{v}_l\,dV + \int_{V'_N}\Delta_l\vec{v}_l\,dV\right), \quad (1)$$

where $V_{PB}$ is the volume of the plateau border and $V'_N$ the volume of half a node; P is the pressure in the liquid, $\rho$ its density, g the gravity, $\eta$ the viscosity, and $v_l$ the local speed of the fluid. All the inertial terms have been neglected, because in all physical situations the Reynolds number is always inferior to one. We distinguished two contributions to the dissipation: a dissipation in the plateau border and a dissipation in the node.

Nondimensionalizing, with $v_\theta$, the average speed in the direction $\mathbf{u}_{PB}$ of the dogbone shapes, making the angle $\theta$ with the vertical, we get

$$(-|\boldsymbol{\nabla}P|+\rho g)\cos(\theta)(V_{PB}+V'_N)$$
$$= \eta v_\theta \times \left\{ \begin{array}{l} \dfrac{r^2(L-\alpha r)}{r^2}\left|\int_{\tilde{V}_{PB}}\tilde{\Delta}_{\perp l}\tilde{\vec{v}}_l\cdot\vec{u}_{PB}\,d\tilde{V}\right| \\[2mm] +\dfrac{r^2(L-\alpha r)}{(L-\alpha r)^2}\left|\int_{\tilde{V}_{PB}}\tilde{\Delta}_{\|l}\tilde{\vec{v}}\cdot\vec{u}_{PB}\,d\tilde{V}\right| \\[2mm] +\dfrac{r^3}{r^2}\left|\int_{\tilde{V}'_N}\tilde{\Delta}_l\tilde{\vec{v}}_l\cdot\vec{u}_{PB}\,d\tilde{V}\right| \end{array} \right\}, \quad (2)$$

where we separated the transversal and longitudinal dissipations in the plateau border, respectively, in the first and second terms.

Calling the three integrals, respectively, $I_{PB\perp}$, $I_{PB\|}$, and $I_n$, and introducing the liquid fraction

$$\varepsilon = \frac{V_{liq}}{V_{total}} = \frac{12(V_{PB}+V'_N)}{V_k},$$

where $V_k = 8\sqrt{2}L^3$ is the volume of the kelvin cell, made of 12 entire dogbone shapes, we get

$$v_\theta = \frac{2\sqrt{2}}{3}\frac{(-|\boldsymbol{\nabla}P|+\rho g)L^2\varepsilon}{\eta\left\{I_{PB\perp}\left[1-\alpha'\left(\dfrac{a}{L^2}\right)^{1/2}\right]+\left(\dfrac{a}{L^2}\right)^{1/2}I'_n+\dfrac{\dfrac{a}{L^2}}{\left[1-\alpha'\left(\dfrac{a}{L^2}\right)^{1/2}\right]}I'_{PB\|}\right\}}\cos(\theta), \quad (3)$$

with $\alpha' = \alpha/\sqrt{\delta_a} \approx 5.8$, $I'_n = I_n/\sqrt{\delta_a}$, and $I'_{PB\|} = I_{PB\|}/\delta_a$.

The integrated flow rate then is $Q = \int_0^{1/2}v_\theta\bar{a}n(\theta)d\theta$ where $\bar{a} = (V_{PB}+\frac{1}{2}V_N)/L$ is the averaged section of the dogbone shapes and $n(\theta)$ the number of dogbone shapes of angle $\theta$ with the vertical intersecting the horizontal plane of surface S. With $n(\theta) = (3/2\sqrt{2})(S/L^2)\cos(\theta)\sin(\theta)$, and averaging over all the orientations, we get

$$Q = \frac{2\sqrt{2}}{3}\frac{(-|\boldsymbol{\nabla}P|+\rho g)L^2S\varepsilon^2}{3\eta\left\{I_{PB\perp}\left[1-\alpha'\left(\dfrac{a}{L^2}\right)^{1/2}\right]+\left(\dfrac{a}{L^2}\right)^{1/2}I'_n+\dfrac{\dfrac{a}{L^2}}{\left(1-\alpha'\sqrt{\dfrac{a}{L^2}}\right)}I'_{PB\|}\right\}}. \quad (4)$$

This equation links the flow rate of water to the size and length of the plateau borders. As to compare this general model and experimental data, numerical values of $I_{PB\perp}$, $I'_n$, and $I'_{PB\|}$ are needed.

Leonard and Lemlich [4], and later Peters [7], found by simulations that, in the case of rigid interfaces, with $v=0$ on the borders of the dogbone shapes: $I_{PB\perp}=K=49.699$. This is, however, not valid if the surface viscosity $\eta_s$ of

the surfactant monolayer is finite. Leonard and Lemlich [4] and Desaï and Kumar [2], have shown numerically that the flow was simply accelerated with an acceleration coefficient $\beta(a)$, which is a function of the ratio $\eta\sqrt{a}/\eta_s$, represented on Fig. 2. There is no analytical expression of $\beta(a)$; however, as to compare later theory and experiments, we used the following fit of $\beta(a)$, shown by the curve on Fig. 2:
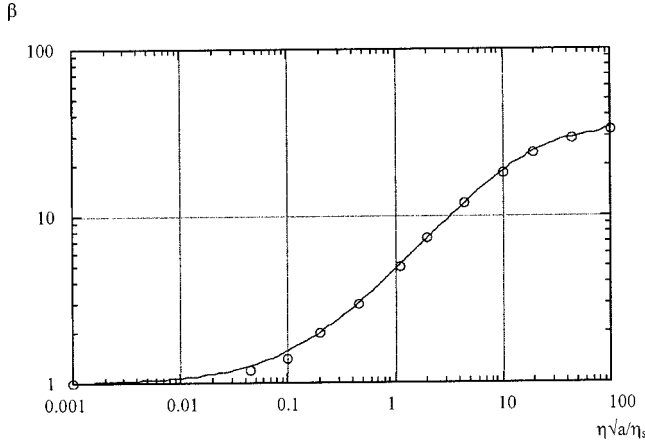
FIG. 2. Evolution of the acceleration coefficient $\beta(a)$ defined by Leonard and Lemlich, and Desaï and Kumar. $\eta$ is the viscosity of the soap solution, $\eta_s$ the surface viscosity of the surfactant monolayer, and $a$ a plateau border section. The dots come from the numerical results of Desaï and Kumar and the curve is the analytical expression $\beta(a)=1+10.9\,\eta/\eta_S\sqrt{a}+6.2(\eta/\eta_S)^{4/3}a^{2/3}-12.5(\eta/\eta_S)^{5/4}a^{5/8}$.

$$\beta(a)=1+10.9\frac{\eta}{\eta_S}\sqrt{a}+6.2\left(\frac{\eta}{\eta_S}\right)^{4/3}a^{2/3}-12.5\left(\frac{\eta}{\eta_S}\right)^{5/4}a^{5/8}. \tag{5}$$

Then $I_{\mathrm{PB}\perp}=K/\beta(a)$.

Recently, Cox et al. [14] modeled numerically the node effect. They found that $I_n'$ could vary between 121 in the case of an infinite surface viscosity and $250\pm25$ in the case of a very low one, which is coherent with the original rough estimation of Koehler et al. based upon the flow through a packed bed of rigid spheres [13] that had given $I_n'\approx400$. Experimentally, the values found by Koehler et al. [12] are comprised between 100 and 300.

From experimental measurements, the longitudinal contribution $I_{\mathrm{PB}\parallel}'$ seems irrelevant and we will then always neglect it.

Finally, let us express the pressure gradient term

$$P_{\mathrm{liq}}(z)=P_{\mathrm{gas}}(z)-\frac{\sigma}{r(z)}=P_0+\rho g\int_z^H\varepsilon(\zeta)d\zeta-\frac{\sigma}{r(z)}$$

$$=P_0+\rho g\int_z^H\varepsilon(\zeta)d\zeta-\frac{\sigma\sqrt{\delta_a}}{\sqrt{a(z)}}, \tag{6}$$

where $P_{\mathrm{liq}}$ is the pressure of the liquid inside the dogbone shapes, $P_{\mathrm{gas}}$ is the pressure inside the bubbles, varying with the height because of the weight of the foam, $\sigma$ the surface tension, $z$ the vertical position, $H$ the height of the foam, and $P_0$ the pressure of the gas inside the upper bubbles.

We obtain the following expression of the flow rate as a function of $a/L^2$, in the region where the capillary rise is negligible:

$$Q=\frac{2\sqrt{2}}{3}\frac{\rho g(1-\varepsilon)L^2S\varepsilon^2}{3\,\eta\left\{\dfrac{K}{\beta(a)}\left[1-\alpha'\left(\dfrac{a}{L^2}\right)^{1/2}\right]+\left(\dfrac{a}{L^2}\right)^{1/2}I_n'\right\}}, \tag{7}$$

where the liquid fraction expression of Phelan et al. [15] is

$$\varepsilon=\frac{a}{L^2}\left[1.06+3.98\left(\frac{a}{L^2}\right)^{1/2}\right]. \tag{8}$$

Two extreme regimes are predicted by this theory. At high liquid fractions $\beta(a)$ is large, the flow is pluglike in the plateau borders and the dissipation occurs mainly in the nodes. Then, $Q$ varies as $\varepsilon^{1.5}$. At small liquid fractions, the volume of the nodes is small and the flow is slowed down in the plateau borders. $Q$ varies as $\beta(\varepsilon)\times\varepsilon^2$, which makes it roughly varying between $\varepsilon^2$ and $\varepsilon^{2.5}$. The transition between these two regimes is clearly ruled by surface viscosity.

One way of testing this model is to impose a continuous flow rate $Q$ to the foam and then measure the stationary liquid fraction $\varepsilon$: this experiment is called steady drainage. Another way we used is to prepare the foam in steady drainage and, at $t=0$, to stop wetting and to follow the releasing of water in time: this is called free drainage. In free drainage, we follow at a fixed height the evolution of the liquid fraction in time. This evolution is linked to the flow equation (7) through a mass conservation equation,

$$\frac{\partial\varepsilon}{\partial t}+\frac{\partial(Q/S)}{\partial z}=0, \tag{9}$$

where $z$ is the vertical coordinate directed downward, and $t$ the time. For example, if Eq. (7) can be approximated by a power law of the kind: $Q\propto\varepsilon^{\alpha+1}$, then this implies that the liquid fraction will decrease according to the power law: $\varepsilon\propto t^{1/\alpha}$. Free drainage is thus another way of testing the drainage theories.

### III. MATERIALS AND METHODS

Foams of SDBS (sodium dodecyl benzene sulfonate) and Dawn® were made; SDBS was purchased at Aldrich and used as received; Dawn® is commercial soap and was used as received. The foaming solutions of SDBS 0.1% w/w and Dawn® 1% w/w were prepared with deionized water.

The experimental setup [9] is presented in Fig. 3.

#### A. Fabrication and characterization of the foam

Foam is made by bubbling perfluorohexane saturated nitrogen through a capillary (hole diameter: 1, 0.5, 0.2, and 0.1 mm) or a porous glass disk (porosity: 150–200, 90–150, and 40–90 $\mu$m) into the foaming solution, inside a Plexiglas column ($25\times25\times60$ cm$^3$). The foam is wetted from above with the foaming solution using a peristaltic pump, at constant rates varying from 0.01 to 1000 $\mu$l s$^{-1}$.

Determination of the foam size is made by image analysis of the channels on the border of the column. Statistics are made over 50 plateau borders. The average length of the
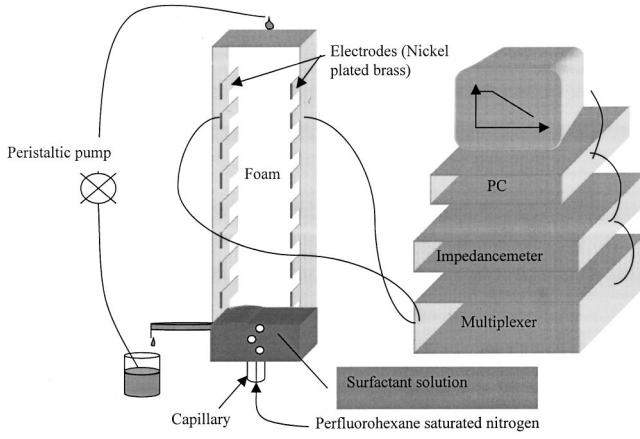
FIG. 3. Foam conductivity apparatus.

plateau border in volume $L_{PB}$ can be calculated from the average length of the parietal plateau borders $L_{PBP}$, from the work of Cheng and Lemlich [16]. For size dispersions, defined as the ratio of the standard deviation [17] over the average, of the order of 30%, like the ones we have, we can deduce that $L_{PB}=L_{PBP}/1.2$, where $L_{PBP}$ is the average length of the parietal plateau borders [18].

Bubbling is stopped during the experiments. The foams studied are stable: no coalescence occurs during the whole experiment, and Ostwald ripening is stopped by the perfluorohexane [19], which allows us to study for a few hours fine foams with parietal plateau borders $L_{PBP}$ as small as 0.24 mm.

All the interfaces are supposed saturated with surfactant and the surfactant concentrations are considered sufficiently high so that the kinetics of adsorption and desorption be fast enough to erase any concentration gradient, according to the work of Stoyanov *et al.* [20]. The foam reposes on the foaming solution and is 50 cm high. The room is thermostated at 21 °C.

### B. Liquid fraction measurements

The liquid fraction is measured in two ways: conductivity and weight.

### 1. Conductivity

The conductivity method has long been used to measure the liquid fraction of foams, and, compared to other methods, it has the advantage of measuring accurately liquid fractions as low as $10^{-5}$.

Lemlich and co-workers [21–23], and Peters [7] gave extensive validations of the method; Phelan *et al.* [15], in 1996, gave the latest relationship between the conductivity of the foam and its liquid fraction, which we used in our study

$$\frac{a}{L^2} \approx \sqrt{2}\{[(3.17K)^2+\sqrt{2}K]^{1/2}-3.17K\}^2, \qquad (10)$$

where $K$ is the relative conductivity of the foam $K=Z_0/Z$, $Z_0$ being the resistance of the foaming solution, and $Z$ the foam resistance. In its model, Phelan *et al.* take into account

the water contained in both the channels and in the nodes, considering the films negligible. According to the authors, it is valid for $\varepsilon<7\%$.

The apparatus we use is made of 25 nickel plated brass electrodes ($1.5\times2$ cm$^2$) with their counterelectrodes, uniformly distributed along two opposite sides of a column of square section. Each couple of electrode is connected to a multiplexer that sends the chosen channel to an impedancemeter; a PC controls the two apparatuses and allows for the programming of various measurement processes. The frequency of the signal is automatically adapted as to measure pure conductivity, and is chosen to be the lowest frequency at which the phase is within $\pm1°$. Typically, it varies between 100 and 1000 Hz.

This method has the advantages of being a local investigation of the liquid fraction, and of giving accurate measurements. Its drawback is the need for a model that has to be tested.

We calibrated our conductivity apparatus using a front propagation measurement. The front propagation measurement is a direct measurement of the liquid fraction through the measurement of the speed of the flow $v_1$ at an imposed flow rate $Q_1$,

$$\varepsilon=\frac{Q_1}{S v_1}, \qquad (11)$$

where $S$ is the container section.

This method has long been used under the name of forced drainage. However, to avoid possible dissipative effects of strong liquid fraction gradients [24], and so as to reach liquid fractions as low as possible, we modified the method using small fronts.

In our method, we prepare a foam under constant wetting with a flow rate $Q_1$, and, at time zero, we increase suddenly the flow rate at $Q_2=Q_1\times\alpha$ where $\alpha$ is a constant close to one; we chose $\alpha=1.5$. A small front then propagates down the foam with a speed $v_f$ that is a function of the two flow rates $Q_1$ and $Q_2$. Successive measurements are made keeping the ratio $\alpha=Q_2/Q_1$ constant.

Making the hypothesis that $Q\propto\varepsilon^\chi$, then $v_1$ can be deduced from $v_f$ following (see the Appendix for detailed calculus): $v_f=[(\alpha-1)/(\alpha^{1/\chi}-1)]v_1$. The value of the power law $\chi$ is given by the computation of $Q_1$ vs $Q_1/Sv_f$. Finally, the liquid fraction is deduced using the relationship (11). To get $v_f$, we measure the conductivity at a known distance $\zeta$ from the top of the foam; we visualize a jump in conductivity and report the time $t_f$ corresponding to the middle of the jump. Then $v_f=\zeta/t_f$.

The results of the calibration are given on Fig. 4. The conductivity measurements interpreted with the model of Phelan *et al.* give results perfectly compatible with the front velocity measurements, for liquid fractions varying at least between 0.4% and 4%. Note that the last points for each curve are probably false, because the bubbles begin to move. These results are compatible with those found in the literature [15].

Liquid fraction from conductivity measurements
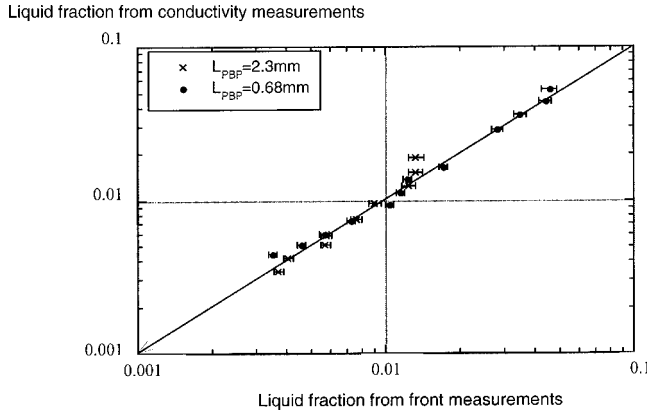


FIG. 4. Calibration of the conductivity. Liquid fraction deduced from conductivity measurements through the equation of Phelan *et al.* vs liquid fraction deduced from front propagation measurements. Two bubble sizes given in terms of average parietal plateau border length $L_{PBP}$. The straight line gives the perfect agreement.

### 2. Hydrostatic weight

Another way of measuring the liquid fraction of the foam is to weight it. The method we use is schematized on Fig. 5. A constant flux is imposed to the column that has an overflow pipe at its bottom. The level of the water will stabilize at an height $h_1$, a bit above the height of the overflow pipe exit, the more so, the higher the flow rate. We then impose the same flux to the foam and measure the stationary height $h_2 < h_1$ of the water level, on which the foam sits. The height of water contained in the whole foam is $h_1 - h_2$. The liquid fraction of the foam is thus $\varepsilon = (h_1 - h_2)/H$, where $H$ is the foam height. The condition for this measurement to be valid is that there be no sticking of the foam on the container sides. This can be tested by wetting the foam, stopping the wetting and let it drain, and then wet it again at the same flow rate. If the water level recovers its initial value, there is no sticking. Experimentally, for SDBS 0.1%, this is true for liquid fractions above 3%. Let us note that this method is not valid for sticking surfactants such as proteins.
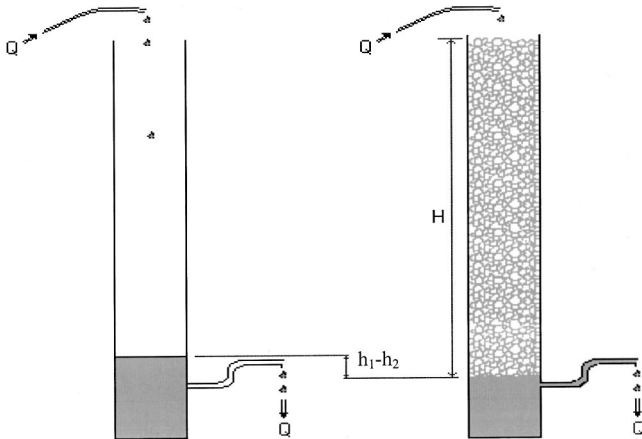


FIG. 5. Weight measurement method. $h_1$ is the level of water without foam and $h_2$ the level of the water with the foam; $H$ is the total height of the foam. The average liquid fraction in the whole foam is $(h_1 - h_2)/H$.

Flow rate/Column section (mm/2)
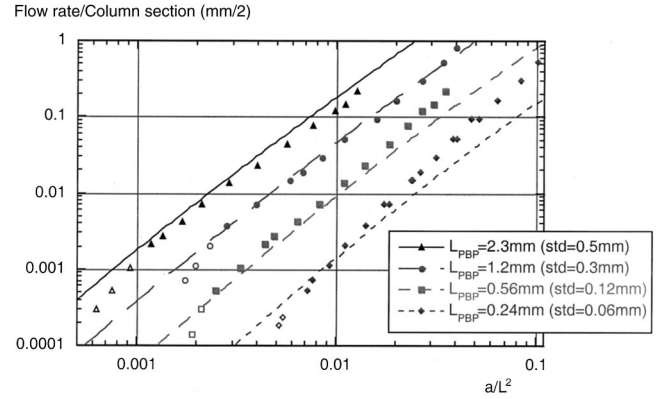


FIG. 6. Steady drainage experiments, $Q$ vs $a/L^2$. $a/L^2$ is deduced from conductivity measurements ($\varepsilon < 5\%$) and weight measurements ($\varepsilon > 4\%$). Foaming solution, SDBS 0.1%, for four bubble sizes given in terms of average parietal plateau border length $L_{PBP}$. The open symbols correspond to cases where the capillary rise intervenes, which we will not consider here. The lines represent the best fit of Eq. (7) with the values $\rho = 10^3$ kg m$^{-3}$, $g = 9.81$ m s$^{-2}$, and $\eta = 1$ cP. The values found for the two free parameters $\eta_s$ and $I'_n$ are $I'_n = 100 \pm 25$ and $\eta_s = 3 \times 10^{-5} \pm 10^{-5}$ cP m.

The disadvantage of this method is that it is a measurement of the average liquid fraction in the whole foam, taking into account the lowest part of the foam that is wetter because of the capillary rise. It can, however, be shown that the capillary rise has a negligible effect when $\varepsilon \gg 0.4\%$. $\varepsilon$ corresponds thus to the local liquid fraction $\varepsilon(z)$, when the liquid fraction is homogeneous, i.e., is independent on the height, which is the case in steady drainage, and when $\varepsilon \gg 0.4\%$.

Here, we have used the weight measurement when $\varepsilon \geq 4\%$; with our method the typical precision obtained is of $\pm 0.3\%$.

### IV. EXPERIMENTS

Figure 6 shows the steady drainage experiments given as the evolution of the flow rate normalized by the column section, with the ratio $a/L^2$. We studied four bubble sizes. They are estimated in terms of mean parietal plateau border length $L_{PBP}$ and the corresponding standard deviation (std). The filled symbols represent the conductivity and hydrostatic data, the errors on the measurements are of the order of the dot size ($<5\%$). The open symbols are the cases where the capillary rise is no more negligible, and which we will not consider in this study. The lines represent the generalized theory (7) with the values: $\rho = 10^3$ kg m$^{-3}$, $g = 9.81$ m s$^{-2}$, and $\eta = 1$ cP. The values found for the two free parameters $\eta_s$ and $I'_n$ are: $I'_n = 100 \pm 25$ and $\eta_s = 3 \times 10^{-5} \pm 10^{-5}$ cP m. They are compatible with those found in the literature [10,14].

First of all, we see that for the biggest bubbles ($L_{PBP} = 2.3$ and 1.2 mm), the experiments agree with the theory; noticeably, we can find the two extreme regimes predicted by the theory. At high liquid fractions ($\varepsilon > 1\%$), the node dissipation dominates and $Q$ follows: $Q \propto (a/L^2)^{1.7}$ which is
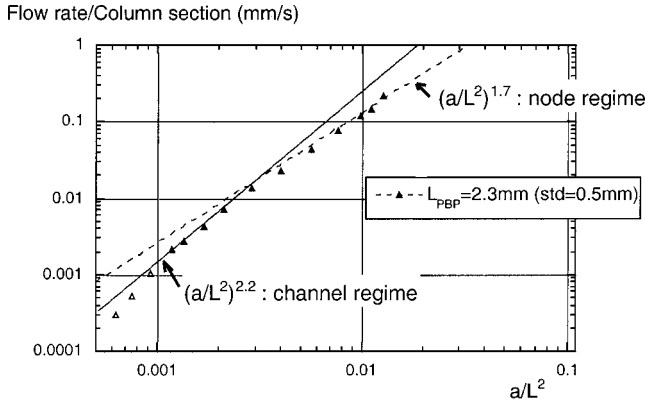
FIG. 7. Steady drainage experiments, $Q$ vs $a/L^2$. $a/L^2$ is deduced from conductivity measurements. Foaming solution, SDBS 0.1%; average parietal plateau border length $L_{PBP}=2.3$ mm. The open symbols correspond to cases where the capillary rise intervenes, which we will not consider here. The dashed line corresponds to the power law predicted by the node theory [$Q \propto (a/L^2)^{1.7}$], and the full line, the power law predicted by the channel theory [$Q \propto (a/L^2)^{2.2}$]. As predicted by the generalized theory, the node regime is met at high liquid fractions and the channel regime, at low liquid fraction.

close to $Q \propto \varepsilon^{1.5}$; at low liquid fractions ($0.1\% < \varepsilon < 1\%$), the channel dissipation dominates and we have: $Q \propto (a/L^2)^{2.2} \Leftrightarrow Q \propto \varepsilon^2$. This is represented in Fig. 7, where the data of the biggest bubbles are reported, with the dashed line showing the power law predicted by the node theory, and the full line, the power law predicted by the channel theory.

On the other hand, for smaller bubbles ($L_{PBP}=0.56$ and 0.24 mm), we can note an increasing disagreement with the theoretical predictions: at high liquid fractions first the flow seems enhanced the more so the smaller the bubbles. For the foam at $L_{PBP}=0.24$ mm the whole curve follows the power law $Q \propto (a/L^2)^{2.6}$.

Thus, the main demonstration of these data is that the drainage behavior depends strongly on the bubble size: the power law linking the flow rate and the liquid fraction (or $a/L^2$) depends on the bubble size, contrarily to what is predicted by the existing theories. This phenomenon is confirmed by the free drainage experiments presented in Fig. 8. As already mentioned, the free drainage is also a method to test the drainage theory. We see that the liquid fraction decreases as the inverse of square time: $\varepsilon \propto t^{-2}$ only for big bubbles; for smaller bubbles, the power law is closer to $\varepsilon \propto t^{-1}$ because the "nodes" regime is overlapped. The power laws, here also, evolve with the bubble size. Moreover, the exponents deduced from free drainage experiments are compatible with the one found in steady drainage: Table I. These data are reproducible; moreover, same experiments with Dawn® soap gave the same behavior.

## V. DISCUSSION

Many possible explanations have been studied among which: a change of morphology, an effect of surface viscosity, and an effect of the walls of the cell.

At high liquid fractions, the nodes get bigger than the
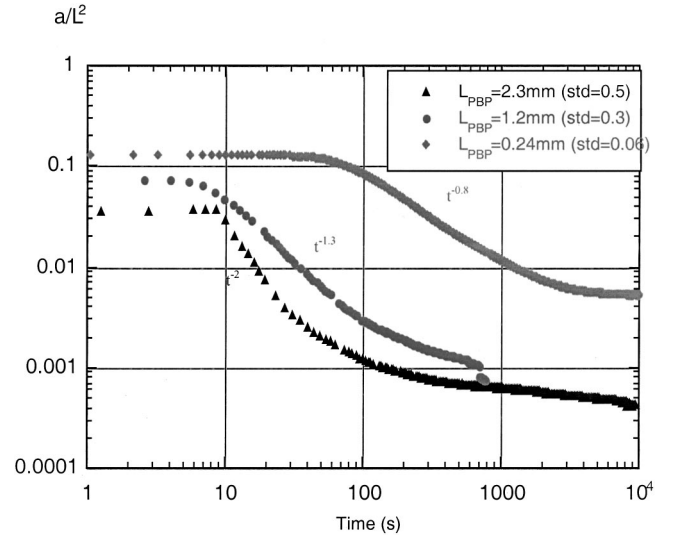


FIG. 8. Free drainage experiments: $a/L^2$ vs time. $a/L^2$ is deduced from conductivity measurements. Foaming solution: SDBS 0.1%. Three bubble sizes are given in terms of average parietal plateau border length $L_{PBP}$.

plateau borders and one may explain the disagreement between our data and the theory by this change of morphology. We recall that Eq. (2) is restricted to small liquid fraction and in the theoretical limit where the channels have disappeared modifications must be introduced. In this case, at high liquid fraction a power law $Q \propto (a/L^2)^{2.2} (\Leftrightarrow Q \propto \varepsilon^2)$ can be expected. However, this would always happen for a critical liquid fraction, independent of $L$, which is not what is observed. Since the drainage behavior can not be described by the liquid fraction only, there must thus be another typical size.

The influence of three characteristic sizes of the system have been studied and detailed here: the ratio $\eta_s/\eta$, the container size, and the film thickness.

$\eta_s/\eta$ is a characteristic size existing in the model. There is, as shown by the study of Cox *et al.*, an effect of the surface viscosity in $I'_n$. This dependence may change the power law. However, the change in $I'_n$, which is only of a factor of two between the two cases $\eta_s/\eta \to 0$ and $\eta_s/\eta \to \infty$ appears to be too low to explain the flow enhancement by a factor of 5 seen for the smaller bubbles, at high liquid fractions.

The column dimension is another obvious characteristic size of the system. Indeed, the channels at the walls of the

TABLE I. Exponents of power laws of drainage deduced from steady drainage and free drainage, for various bubble sizes, given in terms of average parietal plateau border length $L_{PBP}$. SDBS 0.1%.

| Value of $\alpha$ (mm) | Steady drainage $Q \propto \varepsilon^{a+1}$ | Free drainage $\varepsilon \propto t^{1/a}$ |
| --- | --- | --- |
| $L_{PBP}=2.3$ (std=0.5) | 1.7 | 1.5 |
| $L_{PBP}=1.2$ (std=0.3) | 1.8 | 1.8 |
| $L_{PBP}=0.24$ (std=0.06) | 2.2 | 2.1 |
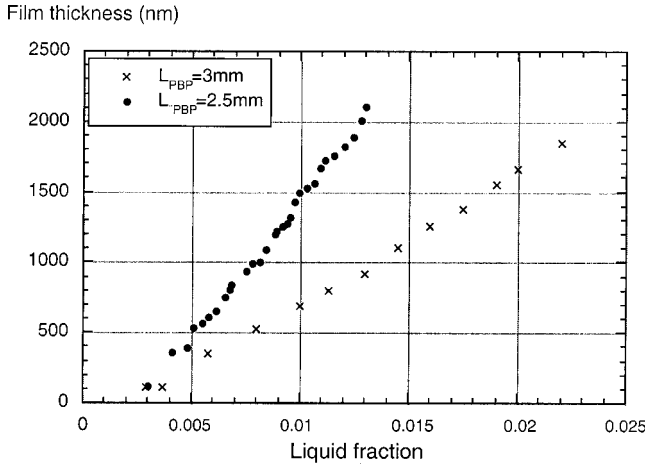
FIG. 9. Vertical film thickness vs liquid fraction. The liquid fraction is measured by conductivity. SDBS 0.1%. $L_{PBP}=2.5$ and 3 mm.



FIG. 10. Pattern of flow inside the films.

column are bigger than the ones in the bulk, moreover, they form a two-dimensional (2D) network, which consequently brakes less the flow than a 3D network. We then studied the effect of the walls of the column, but showed that this could not explain this enhancement of the flow [18,24]: experimentally, the drainage does not change with the container size.

### A film contribution?

Finally, another characteristic size in the system, which has been neglected until now is the film thickness. We then tried to see whether the films could have an influence on the drainage or not, by measuring their thickness in the foam, during a steady drainage experiment and by seeing their evolution with the flow rate.

For this data we used classical light interference measurements. In a black room, the foam is enlightened with a white light directed by a fiber optic to the normal of a vertical film inside the foam. The reflected light is collected through a beam splitter, sent to a grating, which gives in turn the spectra of the reflected light. The film thickness $d$ is then given by the Bragg law: $2nd=(m+\frac{1}{2})\lambda$, where $n$ is the refractive index of the water, $\lambda$ the wavelength, and $m$ the interference order. The interference order is deduced from the successive interference peaks.

The results are shown in Fig. 9. These measurements have been made on foams of SDBS 0.1% w/w, with $L_{PBP}=2.5$ mm or 3 mm, which is for relatively big bubbles. We see that the films are swollen to more than 2 $\mu$m; at these thicknesses, the films appear white with the pattern of flow shown on Fig. 10, where we see noticeably that the water runs across the film, from the upper node to the lower one. They are actually pinched on the regions in contact with the plateau borders and swollen inside as shown on Fig. 11. This swelling is then obviously due to the flow. The water appears to flow mainly in the center of the film, forming a big trickle. This flow must drag along the surfactant down from the upper part of the film, thus generating a concentration gradient from up to down. It is probably this gradient that causes the
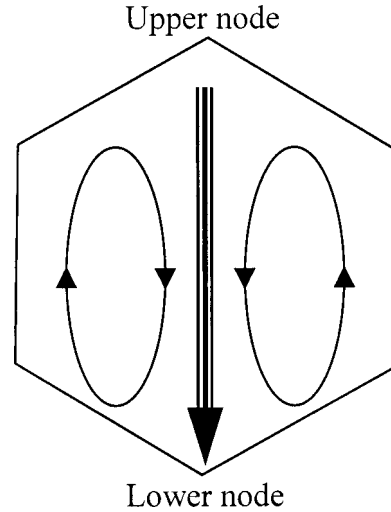
upper flow on the sides. This may thus be close to an effect of marginal regeneration.

The films are then far thicker than usually said: are they still negligible in drainage?

Let us calculate the contribution of the films to the liquid fraction. The average surface $A_f$ occupied by the films on a bubble is [25] $A_f\approx27L_{PB}^2(1-1.52\sqrt{\varepsilon})^2$. Their liquid fraction is thus

$$\varepsilon_f=\frac{\frac{h}{2}A_f}{V_k},$$

where $h$ is the average film thickness, and the total liquid fraction becomes

$$\varepsilon=\frac{a}{L_{PB}^2}\left[1.06+3.98\left(\frac{a}{L_{PB}^2}\right)^{1/2}\right]+1.19\frac{h}{L_{PB}}(1-1.52\sqrt{\varepsilon})^2.$$

For $L_{PBP}=2.5$ mm and $\varepsilon=1.3\%$, if we consider the average films thickness being 2 $\mu$m, the liquid fraction in the films is 0.07%. The liquid fraction in the films is thus negligible for big bubbles. Moreover, the speed of the downward flow inside the films (from node to node) appears to be of the same order of the global speed. Then, their contribution to the overall drainage remains negligible for big bubbles.

What happens for smaller bubbles?
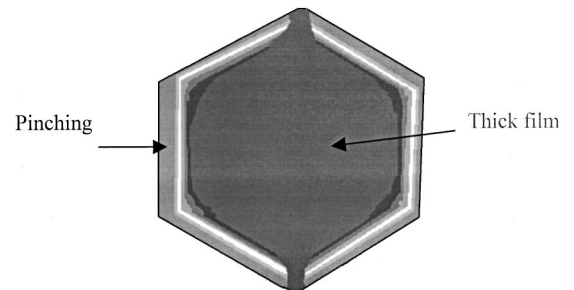


FIG. 11. Pattern of film swelling.

TABLE II. Liquid fraction measured from front propagation measurements and weight measurements in fine foam, of average parietal plateau border length $L_{PBP} = 0.33$ mm. SDBS 0.1%.

| Liquid fraction from weight measurements (%) | Liquid fraction from front propagation measurements (%) |
|---|---|
| $1.8 \pm 0.3$ | $3.2 \pm 0.3$ |
| $3.2 \pm 0.3$ | $4.1 \pm 0.4$ |
| $3.9 \pm 0.3$ | $5.3 \pm 0.5$ |
| $4.3 \pm 0.3$ | $6.6 \pm 0.6$ |

Decreasing the size, the colors disappear. The foams with $L < 1$ mm are almost always white. In the case where $L = 0.3$ mm: colors can be seen for $a/L^2$ around 1%, in a very short domain. These colors seem to correspond to thickness around 400 nm. After this region, the films get white with visible water circulation like Fig. 10.

We believe the transition between thin and thick films to be steeper in fine foams than in big foams, and the films to be thicker than 2 $\mu$m for $a/L^2$ exceeding 2% (for $L = 0.3$ mm). The liquid fraction in the films would then be 0.4%, which is no more negligible. The films may then intervene in drainage by increasing the porosity and changing the flow boundary conditions.

Another proof of a possible non-negligible swelling of the films in fine foams is the following. In Table II, we compare the liquid fraction deduced from front measurements and the one deduced from weight measurements in fine foams. We see that the front method measures highest values than the weight. This can be due to a swelling of the films induced by the flow: thus the vertical films are thicker than the horizontal ones, and the front speed is enhanced. This implication of the films swelling on liquid fraction measurement methods will be dealt with in details elsewhere [26].

Another important implication of the film swelling, is that the flow conditions, notably in the nodes, are changed, which implies a dependence, which could be strong, of the node constant $I'_n$ with the liquid fraction.

Numerous authors have tried to model the drainage of films during free drainage [3,6]; however, it has always been modeled as axisymmetric drainage, with only water flowing from the films towards the plateau borders, which seems to us qualitatively and quantitatively different to what we show here: the water clearly runs across the films from node to node, in a nonaxisymmetric way. Before modeling the drainage taking into account a film contribution, we believe it is necessary to understand first the way the water flows through the films, and simply: why?

## VI. CONCLUSION

We have measured the drainage of foams of varying sizes: the parietal plateau borders lengths running from 0.24 to 2.4 mm. We show that for big bubbles, the generalized theory of Koehler *et al.*, taking into account the work of Leonard and Lemlich and Desaï and Kumar on the acceleration due to the finite surface viscosity of the surfactant, explains well the experiments. The two extreme dissipation effects are found,
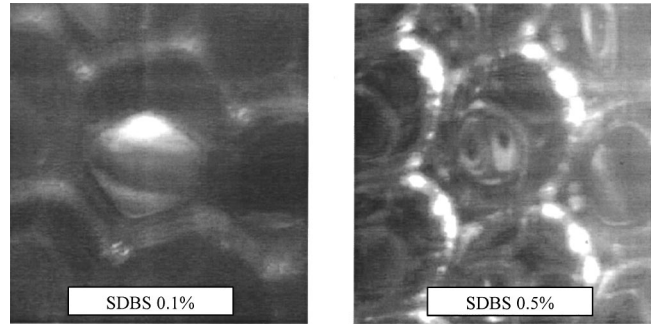


FIG. 12. Patterns of films inside foams of SDBS 0.1% and 0.5%.

with, at high liquid fractions, the node dissipation dominating, and, at low liquid fractions, the channel dissipation.

However, decreasing the size of the bubbles, the power law linking the flow rate to the liquid fraction unexpectedly increases, at high liquid fractions at first, and for all the liquid fractions for the finer foams.

Measurements of film thickness *in situ*, in foams under steady drainage, show that the vertical films can reach thickness over 2 $\mu$m, which is far more than is usually considered. The films are swollen inside and pinched on their sides, and strong water circulation can be seen, with a noticeable flow from the upper node to the lower node, at the speed of the overall flow. We show that the films may be also that thick in fine foams; which in turn would make them no longer negligible both in their contributions to the liquid fraction and to the draining rate.

Consequences of this film swelling are, first, that the flow conditions in the nodes are expected to change with the swelling, second, that the liquid fraction measurements can lead to false results if the films are neglected, third, that the porosity of the foam increases, and fourth, that the isotropy of the foam is now broken.

Finally, we would like to point out that the swelling of the films we present is still misunderstood. It seems noticeably to depend strongly on the physical and chemical characteristics of the surfactant solution. As an illustration, we show in Fig. 12 two pictures of vertical films in foams under steady drainage. If the films of SDBS 0.1% are swollen rather uniformly, the films at SDBS 0.5% have instead two black eyes on each side, showing a different water circulation pattern. We thus feel that this phenomenon of swelling remains entirely to be understood.

It raises a lot of open questions and problems: how to describe the hydrodynamic interaction in thick films and the evolution with the liquid fraction? How to quantify the flow inside one film, taking into account the surface viscosity effect? What is the influence of the nature of the surfactant solution on the swelling? How to model foam drainage with these new parameters?

## APPENDIX: EXPRESSION OF THE FRONT SPEED

When a front propagates down a foam, the flow rate can be written as

$$Q = Q_1 + (Q_2 - Q_1)H(\nu_f t - z), \tag{A1}$$

where $Q_1$ is the initial wetting flow rate, $Q_2 > Q_1$ is the final wetting flow rate, $z$ the vertical ordinate, increasing downward and being zero at the top limit of the foam, $\nu_f$ the front speed and $t$ the time. $H$ is the Heaviside function. As well, the liquid fraction is

$$\varepsilon = \varepsilon_1 + (\varepsilon_2 - \varepsilon_1)H(\nu_f t - z), \tag{A2}$$

where $\varepsilon_1$ is the initial liquid fraction, $\varepsilon_2 > \varepsilon_1$ is the final liquid fraction.

The mass conservation equation writes

$$\frac{\partial \varepsilon}{\partial t} + \frac{\partial (Q/S)}{\partial z} = 0, \tag{A3}$$

where $S$ is the column section. It leads to

$$\nu_f(\varepsilon_2 - \varepsilon_1) - \frac{Q_2 - Q_1}{S} = 0 \Leftrightarrow \nu_f = \frac{Q_1}{S\varepsilon_1}\frac{Q_2/Q_1 - 1}{\varepsilon_2/\varepsilon_1 - 1}. \tag{A4}$$

In our method we keep the ratio $Q_2/Q_1 = \alpha$ constant. Making the approximation: $Q \propto \varepsilon^\chi$, with $\chi$ constant, we get the link between the front speed and the fluid velocity $v_1$ at the flow rate $Q_1$,

$$\nu_f = v_1\frac{\alpha - 1}{\alpha^{1/\chi} - 1}. \tag{A5}$$

[1] G. D. Miles, L. Shedlovsky, and J. Ross, J. Phys. Chem. **49**, 93 (1945).

[2] D. Desai and R. Kumar, Chem. Eng. Sci. **37**, 1361 (1982).

[3] A. M. Kraynik, Sandia National Laboratories Report No. 83-0844, 1983 (unpublished).

[4] R. A. Leonard and R. Lemlich, AIChE. J. **11**, 18 (1965).

[5] D. Weaire, N. Pittet, and S. Hutzler, Phys. Rev. Lett. **71**, 2670 (1993).

[6] M. V. Ramani, R. Kumar, and K. S. Gandhi, Chem. Eng. Sci. **48**, 455 (1993).

[7] E. A. J. F. Peters, Master thesis, Eindhoven University of Technology, 1995.

[8] A. Bhakta and E. Ruckenstein, Langmuir **11**, 1486 (1995).

[9] G. Verbist, D. Weaire, and A. M. Kraynik, J. Phys.: Condens. Matter **8**, 3715 (1996).

[10] D. Weaire, S. Hutzler, G. Verbist, and E. Peters, Adv. Chem. Phys. **102**, 315 (1997).

[11] S. A. Koehler, H. A. Stone, M. P. Brenner, and J. Eggers, Phys. Rev. E **58**, 2097 (1998).

[12] S. A. Koehler, S. Hilgenfeldt, and H. A. Stone, Phys. Rev. Lett. **82**, 4232 (1999).

[13] S. A. Koehler, S. Hilgenfeldt, and H. A. Stone, Langmuir **16**, 6327 (2000).

[14] S. J. Cox, G. Bradley, S. Hutzler, and D. Weaire, J. Phys.: Condens. Matter **13**, 4863 (2001).

[15] R. Phelan, D. Weaire, E. A. J. F. Peters, and G. Verbist, J. Phys.: Condens. Matter **8**, 475 (1996).

[16] H. C. Cheng and R. Lemlich, Ind. Eng. Chem. Fundam. **22**, 105 (1983).

[17] $\text{std} = \sqrt{(\Sigma_1^{(n)} x_i^2 - n\bar{x}^2)/(n-1)}$, where $n$ is the number of data points, $x_i$ a data value and $\bar{x}$ the mean.

[18] V. Carrier and A. Colin (unpublished).

[19] F. G. Gandolfo and H. L. Rosano, J. Colloid Interface Sci. **194**, 31 (1997).

[20] S. Stoyanov, C. Dushkin, D. Langevin, D. Weaire, and G. Verbist, Langmuir **14**, 4663 (1998).

[21] R. Lemlich, J. Colloid Interface Sci. **64**, 107 (1978).

[22] A. K. Agnihotri and R. Lemlich, J. Colloid Interface Sci. **84**, 42 (1981).

[23] A. K. Datye and R. Lemlich, Int. J. Multiphase Flow **9**, 627 (1983).

[24] V. Carrier, Ph.D. thesis, University of Bordeaux I, 2001.

[25] S. Hilgenfeldt, S. A. Koehler, and H. A. Stone, Phys. Rev. Lett. **86**, 4704 (2001).

[26] V. Carrier and A. Colin (unpublished).